# Imaging Facial Signs of Neuro-Physiological Responses

Dvijesh Shastri[1], Arcangelo Merla[2], Panagiotis Tsiamyrtzis[3], Ioannis Pavlidis[1]*

Computational Physiology Lab[1],
Department of Computer Science,
University of Houston, Houston, TX, USA,
djshastr@mail.uh.edu,ipavlidis@uh.edu

ITAB - Institute of Advanced Biomedical Technologies[2],
Department of Clinical Sciences and Bioimaging,
University "G. D'Annunzio",
Chieti, Italy
a.merla@itab.unich.it

Department of Statistics[3],
Athens University of Economics and Business
Athens, Greece
pt@aueb.gr

**Abstract.** In the present paper, we introduce an integrated framework for detecting peripheral sympathetic responses through purely imaging means. The measurements are performed on three facial areas of sympathetic importance, that is, periorbital, supraorbital, and maxillary. To the best of our knowledge, this is the first time that the sympathetic importance of the maxillary area is analyzed. Because the imaging measurements are thermal in nature and are composed of multiple components of variable frequency (i.e., blood flow, sweat gland activation, and breathing), we chose wavelets as the image analysis framework. The image analysis is grounded on GSR signals, which are still considered the golden standard in peripheral neurophysiological and psychophysiological studies. The experimental results show that monitoring of the facial channels yields similar detecting power to GSR's.

## 1 Introduction

The Autonomic Nervous System (ANS) and particularly its sympathetic division has been the object of intense study in neurophysiology and psychophysiology. The sympathetic division readies the body for a crisis that may require sudden, intense physical activity. It is a primal survival mechanism. Therefore, interest on methodologies that scrutinize sympathetic responses is well founded and has many applications.

* To whom all correspondence should be addressed

When sympathetic activation occurs, an individual experiences increased activity in the cardiovascular and respiratory centers of the pons and medulla oblongata, leading to elevations in blood pressure, heart rate, breathing rate, and depth of respiration. These vital sign changes are mediated through adrenergic postganglionic fibers. Determination of sympathetic activation through vital sign monitoring is not always straightforward.

As an alternative, researchers focused their efforts on sympathetic manifestations effected through cholinergic postganglionic fibers. These fibers innervate sweat glands of the skin and the blood vessels to skeletal muscles and the brain. They provide a pathway to stimulating sweat gland secretion and selectively enhancing blood flow to muscles.

In this context, Electro-Dermal Activity (EDA) has been the gold standard for peripheral monitoring of sympathetic responses. EDA is measured through the Galvanic Skin Response (GSR), which is a simple and reproducible method for quantifying sweat gland activation in the palm. Alternatively, EDA can be captured through a palm thermistor, which registers the full thermoregulatory phenomenon including changes both in blood flow and sweat gland activation. In our case, this is a useful yardstick, as it provides palm information similar to the one thermal imaging provides for the face.

Indeed, in recent years, we have demonstrated that during arousal additional physiological signs materialize on the face. Specifically, we have shown that increased blood flow in the periorbital [1][2] and supraorbital [3] areas are ubiquitous manifestations of stress. We have also developed a thermal imaging methodology to extract both the periorbital and supraorbital signals.

In the present paper, we link traditional probe-based with the newer image-based neurophysiological methodologies. We study comparatively the periorbital, supraorbital, and palm channels (GSR and thermistor) within a classic repeated arousal experiment. First, we introduce a novel modeling methodology to quantify the GSR signal and validate the arousal experiment. In addition, we demonstrate that concomitantly to the palm area, strong sweat gland activation is manifested in the maxillary area. This is one more sympathetic thermoregulatory phenomenon manifested on the face. Therefore, it can be sensed and computed through thermal imaging. We apply a wavelets analysis method for all channels (periorbital, supraorbital, maxillary, GSR, and palm thermistor). The results reveal tonic (baseline) and phasic (event related) affinity of the three imaging channels to the GSR and palm thermistor channels. We also identify the presence of a breathing component in the maxillary signal.

Our research brings to the fore the pivotal role of facial physiology in the manifestation of stress and establishes the methodological framework for sensing peripheral sympathetic responses through imaging means.

In the rest of the paper we unveil our new imaging methodology for modeling and analyzing the facial sympathetic channels. Specifically, in section 2, we describe the method itself. In section 3, we report and discuss its experimental validation.

## 2 Methodology for Signal Modeling and Analysis

### 2.1 Modeling of GSR Signal

The first goal is to model the GSR signal and be able to draw inferences about the repeated arousal effect on each subject. This is very important, as GSR is the ground-truth in our studies and validation of ground-truth is a prerequisite for meaningful comparative studies. Specifically, our modeling scheme needs to show that individuals tend to habituate and therefore, GSR amplitudes tend to reduce, latencies tend to increase, and wave-shapes tend to remain unaltered. These well-established and understood patterns of repeated arousals in normal subjects, if quantified here, they will validate our experimental design and execution.

As we will discuss in the Experimentation Section, we stimulate the subjects with 3 auditory startles spaced at least 1 min apart. For this reason, we choose to split the GSR signal in three non-overlapping segments:

- $S1$: 2 sec before first startle until 2 sec before second startle
- $S2$: End of $S1$ to 2 sec before third startle
- $S3$: End of $S2$ to end of experiment

We divide each of the segments $S1$, $S2$, and $S3$ into three subsegments:

- $LS$: The Left Subsegment, which spans from the beginning of the segment till the maximum value (shortly after startle).
- $RS$: The Right Subsegment, which spans from the maximum value till the end of the segment.
- $LSOS$: The Left Stimulus Onset Subsegment, which starts at the time of the startle and lasts until the maximum value is reached. It is portion of $LS$ and is useful in estimating the habituation effect.

The GSR signal around the stimulus is formed by the charging and discharging of an RC circuit, which closes on the palm skin during emotional sweat gland activation. Charging corresponds to arousal ($LS$) and it is characterized by an exponential increase. Discharging corresponds to arousal waning ($RS$) and it follows an exponential decay. For this reason, we choose the Laplace distribution to model the GSR signal. The probability density function is given by:

$$f(t|\mu,\beta) = \frac{1}{2\beta} exp\left(-\frac{|t-\mu|}{\beta}\right), \tag{1}$$

where $\mu$ (mean) denotes the time parameter, while $\beta > 0$ is the scale parameter.

Although, the GSR signal is not symmetric around the local maximum value, the Laplace distribution is. This led us to model separately $LS$ and $RS$ for every segment (see Fig. 1). For $LS$ we fit a truncated Laplace distribution where the $\mu$ parameter is assumed to be known (location of the maximum) and the distribution is censored to the right of the maximum. Similarly, for $RS$ we use a truncated Laplace distribution where the values at the left of the maximum are censored. The goal then is to estimate the scale parameters of the left and right

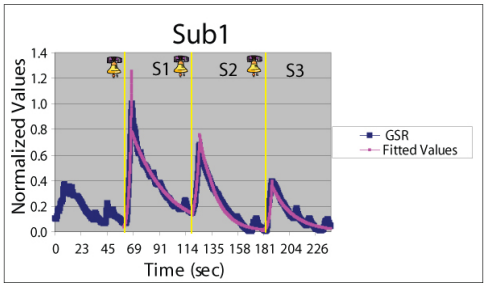


**Fig. 1.** GSR segments $S1$, $S2$, and $S3$ along with the fitted Laplace values for subject Sub1. The stimuli occurrences have been marked appropriately.

distributions (i.e., $\beta_L$ and $\beta_R$). This estimation is done through the Ordinary Least Squares (OLS) method.

For $LS$ where $t \leq \mu$, we have:

$$y = f(t) = \frac{1}{2\beta_L} exp\left(-\frac{\mu - t}{\beta_L}\right) \quad \Rightarrow \quad \ln(y) = \left[-\frac{\mu}{\beta_L} - \ln(2\beta_L)\right] + \frac{1}{\beta_L}t, \qquad (2)$$

so that time $t$ and logarithmic scale $\ln(y)$ are linearly related. We use OLS to estimate the slope, whose inverse is the parameter of interest $\beta_L$.

For $RS$ where $t \geq \mu$, we have:

$$y = f(t) = \frac{1}{2\beta_R} exp\left(-\frac{t - \mu}{\beta_R}\right) \quad \Rightarrow \quad \ln(y) = \left[\frac{\mu}{\beta_R} - \ln(2\beta_R)\right] - \frac{1}{\beta_R}t, \qquad (3)$$

so that time $t$ and logarithmic scale $\ln(y)$ are linearly related. We use OLS to estimate the slope, whose negative inverse is the parameter of interest $\beta_R$.

For $LSOS$ we apply linear (versus exponential) fitting, as these subsegments are nearly impulsive.

### 2.2 Wavelets Analysis of Sympathetic Signals

We extract thermal signals from three facial areas: periorbital, supraorbital, and maxillary. In all three cases the regions of interest are tracked using the coalitional tracking method we reported in [4]. In the periorbital area, the extracted signal is formed from the evolution of the mean thermal footprint of the facial arteriovenous complex. This footprint is segmented via a fuzzy segmentation algorithm, which is seeded in the initial frame with two points in the inner orbital areas (see Fig. 2). On each subsequent frame, the seeds are adjusted with help from the coalitional tracker. In the supraorbital area, the extracted signal is formed from the evolution of the mean thermal footprint of the entire region of interest. In the maxillary area, the extracted signal is formed from the evolution of the mean thermal footprint of the entire region of interest.

The periorbital thermal signal is a correlate of the blood supply to the orbital muscle. The supraorbital thermal signal is a correlate of the blood supply to

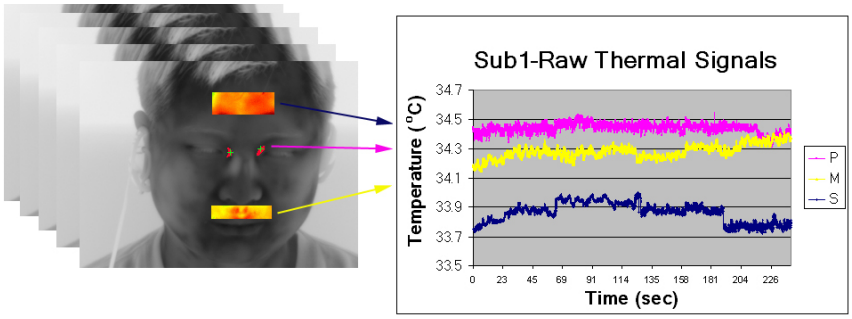


**Fig. 2.** Periorbital, supraorbital, and maxillary regions of interest and the respective mean thermal signals along the timeline. The periorbital measurement is strictly localized on the thermal footprints of the facial artery.

the corrugator muscle. It may also be slightly modulated from the activation of sweat glands in the forehead. The maxillary thermal signal is a correlate of the blood perfusion in the respective area. Based on our observations, it is also heavily modulated from the activation of local sweat glands. Finally, the maxillary signal is periodically modulated from the thermal effect of breathing, due to the proximity of nostrils.

Concomitantly with the three facial imaging signals, we extract palm perspiratory and thermal signals through GSR and thermistor sensors respectively. We also extract the breathing signal through a piezo-respiratory belt transducer. All probe signals (GSR, palm thermistor, and respiratory belt) are synchronized with the thermal imager through an electronic circuit.

The stress content of the GSR signal has been documented in the literature exhaustively [5][6][7]. To associate this content to the facial imaging signals, we use a multi-resolution wavelets approach. The typically noisy profile of facial signals (see Fig. 2) and the confounding phenomena that form them, do not allow direct modeling of their raw waveforms, as in the case of GSR (see Fig. 1). Therefore, component isolation and noise reduction are necessary.

Specifically, we consider that all signals if they are of sympathetic importance they have either a strong phasic or tonic component [8]. The phasic component should be at a scale that matches the inter-stimulus interval of the experiment, while the tonic component will reside at an even higher scale that spans the entire experimental time-line. Any strong extraneous modulation (e.g., breathing) in some signals should be evident in a lower scale (i.e., higher frequency), far away from the phasic and tonic scales.

To quantify the contribution of phasic, tonic, and other components in the signals we apply a Continuous Wavelet Transform (CWT) with a Daubechies-10 mother wavelet. We then compute the energy of each signal in all scales. The energy curves feature global and local maxima. We analyze these maxima to understand if they correspond to phasic or tonic responses. We also compare their relative contributions in each signal.

## 3 Experimentation and Discussion

We used a high quality Thermal Imaging (TI) system for data collection. The centerpiece of the TI system is a ThermoVision SC6000 Mid-Wave Infrared (MWIR) camera [9] (NEDT=0.025°C). We recorded 10 thermal clips from the faces of 10 subjects while resting in an armchair. Concomitantly, we recorded ground-truth GSR, palm thermistor, and piezo-respiratory signals with the PowerLab 8/30, ML870 data acquisition system [10]. The data set features subjects of both genders, different races, and with varying physical characteristics. The subjects were focused on a mental task while they were measured through the thermal imaging and contact sensors. The experiment lasted 4 min. After the first minute the first auditory startle was delivered and after that two more were delivered spaced at least 1 min apart. The experiment ended about 1 min after the delivery of the third startle.

### 3.1 GSR Results

We applied the modeling methodology detailed in Section 2.1 to each segment of every GSR waveform. Therefore, we had 3 segments ($S1$, $S2$, $S3$) $\times$ 3 subsegments ($LS$, $RS$, $LSOS$) $\times$ 10 subjects = 90 cases for which we needed to estimate the scale parameter $\beta$ (Laplace fitting for $LS$ and $RS$) or the slope (linear fitting for $LSOS$). The results are shown in Table 1 and elicit the following conclusions:

- For all stimuli ($S1$, $S2$ and $S3$) $LS$ has a much smaller scale parameter than $RS$ indicating that the phenomenon causes a steep increase and then decays at a much lower rate.
- Comparing the $LS$ parts of $S1$, $S2$, and $S3$, within the same subject, we observe that usually the 1st stimulus causes the steepest increase and as we move to subsequent stimuli the response is less steep (i.e., the $\beta_L$ parameter is increasing).
- Comparing the $RS$ parts of $S1$, $S2$, and $S3$, within the same subject, we observe that usually the subject recovers slowly after the 1st stimulus (i.e., it has a high $\beta_R$ parameter). Recovery from subsequent stimuli is becoming faster (smaller $\beta_R$ parameter).
- Comparing the $LSOS$ parts of $S1$, $S2$, and $S3$, within the same subject, we observe that the estimated (positive) slope of the linear regression is decreasing as we move from $S1$ to $S2$ to $S3$ (habituation).

These conclusions are in accordance with the expected behavior of normal subjects, and therefore our experiment is valid.

### 3.2 Comparative Wavelets Analysis Results

We applied the wavelets analysis methodology detailed in Section 2.2 for all 6 sympathetic signals from all 10 subjects. Fig. 3 shows the wavelet energy curves

| | **Sub1** | **Sub2** | **Sub3** | **Sub4** | **Sub5** | **Sub6** | **Sub7** | **Sub8** | **Sub9** | **Sub10** |
|---|---|---|---|---|---|---|---|---|---|---|
| $S1$-$LS$ | 2.18 | 2.68 | 1.70 | 1.94 | 7.50 | 14.54 | 4.79 | 25.39 | 4.50 | 3.87 |
| $S1$-$LSOS$ | 0.20 | 0.10 | 0.15 | 0.14 | 0.13 | 0.05 | 0.06 | 0.05 | 0.08 | 0.12 |
| $S1$-$RS$ | 30.40 | 33.90 | 27.11 | 40.89 | 36.88 | 82.50 | 151.47 | 38.76 | 68.08 | 25.24 |
| $S2$-$LS$ | 3.75 | 3.04 | 1.77 | 8.49 | 5.69 | 26.16 | 7.89 | 13.13 | 8.29 | 9.37 |
| $S2$-$LSOS$ | 0.11 | 0.07 | 0.13 | 0.08 | 0.12 | 0.03 | 0.10 | 0.04 | 0.10 | 0.11 |
| $S2$-$RS$ | 13.39 | 29.46 | 34.11 | 62.67 | 22.46 | 53.43 | 44.81 | 20.71 | 61.65 | 30.69 |
| $S3$-$LS$ | 1.91 | 2.51 | 2.30 | 10.13 | 2.51 | 62.46 | 15.09 | 2.28 | 10.63 | 5.49 |
| $S3$-$LSOS$ | 0.09 | 0.09 | 0.12 | 0.06 | 0.12 | 0.01 | 0.03 | 0.08 | 0.07 | 0.08 |
| $S3$-$RS$ | 17.93 | 11.36 | 34.25 | 66.67 | 19.12 | 31.53 | 81.62 | 108.44 | 25.21 | 13.44 |

**Table 1.** The estimated $\beta$ parameters for the $LS$ and $RS$ Laplace distributions along with the linear regression slope estimates of $LSOS$.

in lower and higher scales of subject Sub1. In lower scales (i.e., 50-250) the piezo-respiratory signal (Brt) appears to have a dominant component, as it is manifested by the high bell-shaped bulge. This is in accordance with its expected function. The second most prominent component is featured by the maxillary signal (M). This verifies our hypothesis of breathing modulation for this signal, as it is sampled in proximity to the nostrils.

In higher scales, (i.e., 1000-3000) the GSR signal (GSR) appears to have a dominant component, as it is manifested by the high bell-shaped bulge. This is the phasic component as the scale is about 1/3 of the total scale and matches the period of the repeated stimuli in our experiment. The strong presence of a phasic component in the GSR signal is consistent with its nature. The fascinating result here is the almost equally strong phasic component in the maxillary signal (M). This is consistent with our hypothesis of strong sweat gland activation in the maxillary area concomitant to the palm area. Other facial signals (i.e., periorbital-P and supraorbital-S) also have significant but relatively weaker phasic components, which verifies their sympathetic relevance.

At the highest scales that span almost the entire timeline resides the tonic component of the signals. It is worth noting that the GSR signal has the smallest tonic component of all sympathetic channels. This is consistent with the almost unimodal nature of the GSR channel. The maxillary signal (M), which is its facial equivalent, has a much stronger tonic component. In contrast to the GSR signal, the maxillary signal contains not only local sweat gland activation information, but also thermal information related to changes in local blood perfusion. In this sense, the maxillary signal (M) is probably closer to the palm thermistor (Thr) signal.

In general, adrenergic and cholinergic signal components reside in nonoverlapping scales, which makes the adopted multi-resolution approach an ideal analysis tool. The picture emerging from the analysis of the wavelet energy curves for subject Sub1 remains relevant for all the other 9 subjects in our dataset. Fig. 4 shows the mean energy of tonic, phasic, and breathing components of the various sympathetic channels for the entire data set. All the conclusions ex-

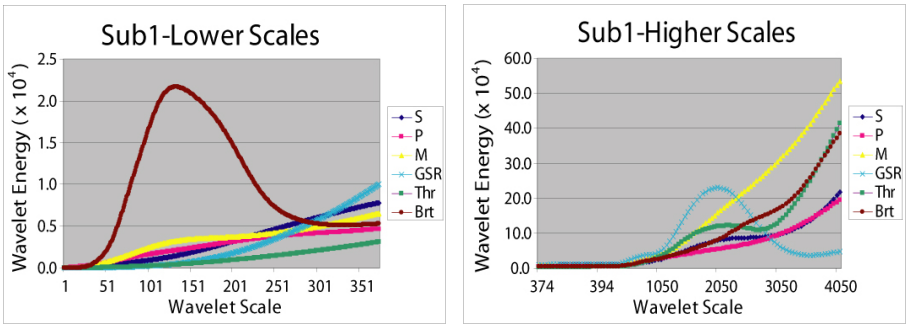


(a) (b)

**Fig. 3.** Wavelet energy curves of subject Sub1 for all 6 sympathetic channels in (a) lower and (b) higher scales.

tracted through the example of subject Sub1 still apply for the thus statistically constructed mean subject.

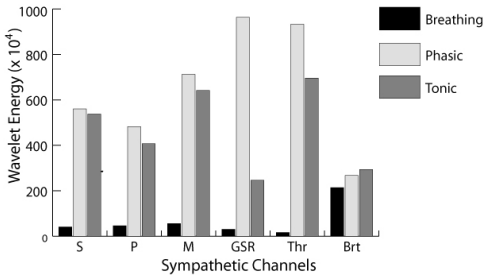


**Fig. 4.** Mean tonic, phasic, and breathing energy components for the various sympathetic channels.

## References

[1] Levine, J., Pavlidis, I., Cooper, M.: The face of fear. The Lancet **357**(9270) (2001) 1757

[2] Pavlidis, I., Eberhardt, N., Levine, J.: Human behavior: Seeing through the face of deception. Nature **415**(6867) (2002) 35

[3] Puri, C., Olson, L., Pavlidis, I., Starren, J.: Stresscam: Non-contact measurement of users' emotional states through thermal imaging. In: Proceedings of the 2005 ACM Conference on Human Factors in Computing Systems (CHI), Portland, Oregon (2005) 1725–8

[4] Dowdall, J., Pavlidis, I., Tsiamyrtzis, P.: Coalitional tracking. Computer Vision and Image Understanding (2007)

[5] Baba, M., Watahiki, Y., Matsunaga, M., Takebe, K.: Sympathetic skin response in healthy man. Electromyography Clinincal Neurophysiology **28** (1988) 277–283
[6] Uncini, A., Pullman, S., Lovelace, R., Gambi, D.: The sympathetic skin response: Normal values, elucidation of afferent components and application limits. The Journal of Neuroscience **87** (1988) 299–306
[7] Elie, B., Guiheneuc, P.: Sympathetic skin response: Normal results in different experimental conditions. Electroencephalogry and Clinical Neurophysiology **76**(258-267) (1990)
[8] Lim, C., Renniea, C., Barry, R., Bahramali, H., Lazzaro, I., Manor, B., Gordon, E.: Decomposing skin conductance into tonic and phasic components. International Journal of Psychophysiology **25** (1997) 97–109
[9] FLIR Systems 70 Castilian Dr., Goleta, California 93117: (http://www.flir.com)
[10] ADInstruments 2205 Executive Circle, Colorado Springs, Colorado 80906: (http://www.adinstruments.com)